Atmospheric
Measurement
Techniques

Background CO$_2$ levels and error analysis from ground-based solar absorption IR measurements in central Mexico

Jorge L. Baylon[1], Wolfgang Stremme[1], Michel Grutter[1], Frank Hase[2], and Thomas Blumenstock[2]

[1]Centro de Ciencias de la Atmósfera, Universidad Nacional Autónoma de México, Mexico City, Mexico
[2]Institute of Meteorology and Climate Research, Karlsruhe Institute of Technology, Karlsruhe, Germany

Correspondence to: Jorge L. Baylon (baylon@atmosfera.unam.mx)

Abstract. In this investigation we analyze two common optical configurations to retrieve CO$_2$ total column amounts from solar absorption infrared spectra. The noise errors using either a KBr or a CaF$_2$ beam splitter, a main component of a Fourier transform infrared spectrometer (FTIR), are quantified in order to assess the relative precisions of the measurements. The configuration using a CaF$_2$ beam splitter, as deployed by the instruments which contribute to the Total Carbon Column Observing Network (TCCON), shows a slightly better precision. However, we show that the precisions in X_{CO_2} ($= 0.2095 \cdot \frac{\text{Total Column CO}_2}{\text{Total Column O}_2}$) retrieved from $> 96\%$ of the spectra measured with a KBr beam splitter fall well below 0.2 %. A bias in X_{CO_2} (KBr $-$ CaF$_2$) of $+0.56 \pm 0.25$ ppm was found when using an independent data set as reference. This value, which corresponds to $+0.14 \pm 0.064\%$, is slightly larger than the mean precisions obtained. A 3-year X_{CO_2} time series from FTIR measurements at the high-altitude site of Altzomoni in central Mexico presents clear annual and diurnal cycles, and a trend of $+2.2$ ppm yr^{-1} could be determined.

1 Introduction

During the last decades, carbon dioxide (CO$_2$) has exceeded the pre-industrial levels by about 40 % mainly due to fossil fuel combustion and land use change (Hartmann et al., 2013), contributing more than any other anthropogenic gas to the positive total radiative forcing of the Earth and becoming the most important anthropogenic greenhouse gas (Myhre et al., 2013). The quantification of the spatial distribution and temporal variation of CO$_2$ sources and sinks can

help to understand the anthropogenic contributions of CO$_2$ to the carbon cycle. This task can be achieved by monitoring the atmosphere using ground-based and satellite observations. Ground-based networks like the Global Atmosphere Watch (WMO, 2014) or the Total Carbon Column Observing Network (TCCON) provide data sets of CO$_2$ concentrations around the world. TCCON is a network of Fourier transform infrared spectrometers (FTIRs) that record solar absorption spectra in the near-infrared (NIR, 3300–13 000 cm^{-1}) spectral region in order to retrieve column-averaged dry-air mole fractions of CO$_2$ (X_{CO_2}) and other molecules that absorb in the NIR (Wunch et al., 2011). TCCON aims to provide reliable, long-term validation data sets for satellite measurements and to improve current knowledge of the carbon cycle. Measurements of CO$_2$ from space have been done by many satellite missions like ACE (Foucher et al., 2011), AIRS (Chahine et al., 2008), IASI (Crevoisier et al., 2009), TES (Kulawik et al., 2010), SCIAMACHY (Reuter et al., 2011), GOSAT (Kuze et al., 2009) and OCO-2 (Wunch et al., 2017), with the last three missions relying on TCCON data for validation.

Studies done to estimate the CO$_2$ concentrations in Mexico City and central Mexico have been scarce, the first one was conducted during 1981 and 1982, in which the diurnal and seasonal variation was estimated taking air samples in different parts of the city (Báez et al., 1988). In two different campaigns (MCMA-2003 and MILAGRO), the CO$_2$ fluxes and concentrations during typical days in the Mexico City metropolitan area (MCMA) were estimated using the eddy covariance technique (Velasco et al., 2005, 2009). The first study using an FTIR was done during September 2001 in the south of the MCMA using a Nicolet Nexus interferom-

eter with a resolution of 0.125 cm^{-1} and retrieving CO$_2$ in the 723–766 cm^{-1} spectral region (Grutter, 2003). From this study the variability and average diurnal cycle of CO$_2$ was recorded with high temporal resolution.

The Altzomoni site is located to the southeast of the MCMA at a height of almost 4000 m a.s.l. (above sea level). Measurements of NIR and MIR (mid-infrared) spectra have been conducted since 2012 using a Bruker IFS 120 and 125 HR. The site has been part of the Network for the Detection of Atmospheric Composition Change (NDACC) since 2015 and has been reporting vertical columns of O$_3$, CO, N$_2$O and CH$_4$ among other gases. As part of the NDACC instrumental configuration, a KBr beam splitter has been used for most of the measurements, but for a limited number of days, a CaF$_2$ beam splitter was also used in order to meet the TCCON instrumental requirements and compare the effect of each configuration in the retrievals of CO$_2$ and O$_2$ as well as in the estimation of X_{CO_2}.

This paper presents X_{CO_2} retrieved from NIR spectra measured from December 2012 to December 2015 in the Altzomoni site and an intercomparison of how the use of KBr and CaF$_2$ beam splitters affect the errors and precision of CO$_2$ and O$_2$ columns and X_{CO_2} mole fractions. Section 2 describes the configuration used in the measurement of the NIR spectra and how these spectra were analyzed for producing the time series of X_{CO_2}. An evaluation of how the used beam splitter influences the total column retrievals and the calculation of X_{CO_2} by means of an estimation of noise errors, precision and bias of each configuration is presented in Sect. 3. The characteristic seasonal and diurnal cycles, as well as the observed trend for this subtropical site in central Mexico, are presented in Sect. 4.

2 FTIR instrument, measurement site and spectral analysis

A high resolution Fourier transform infrared spectrometer (FTIR), Bruker model 120/5 HR, was deployed to measure solar absorption spectra under clear sky conditions. The instrument began operations at a high-altitude location in central Mexico in 2012 as part of a collaboration between the National Autonomous University of Mexico (UNAM) and the Karlsruhe Institute of Technology, and, since 2015, Altzomoni has been part of the Network for the Detection of Atmospheric Composition Change. Routine and remotely operated measurements are performed with a spectral resolution of 0.005 cm^{-1} using a KBr beam splitter, a set of bandpass filters and liquid-nitrogen-cooled mercury–cadmium–telluride and InSb detectors, according to NDACC specifications. The solar tracking is based on the Camtracker system (Gisi et al., 2011) used in other NDACC and TCCON sites and is housed in a dome which can be operated remotely.

Table 1. Microwindows and interfering species used for CO$_2$ and O$_2$ retrievals.

	Microwindows (cm^{-1})	Interfering species
CO$_2$	6180.0–6260.0, 6310.0–6380.0	H$_2$O, CH$_4$
O$_2$	7765.0–8005.0	H$_2$O, CO$_2$

Alternatively, an InGaAs detector is used to record near-infrared (NIR) spectra within each measurement sequence with a resolution of 0.02 cm^{-1}. These NIR spectra, used in this study to retrieve CO$_2$ and O$_2$, were recorded as the average of two scans taken for approximately 38 s with a scanner speed of 40 kHz. In each measurement sequence, a set of six NIR measurements are recorded, taking around 5 min. This small change in solar angles allows the consideration that all measurements belong to the same air mass. A CaF$_2$ beam splitter is also available and was used for a small number of days for the purpose of estimating the noise levels in each optical configuration and how this affects the retrievals.

The FTIR instrument is located at the Altzomoni high-altitude station (19.1187° N, 98.6552° W) located in central Mexico within the Izta-Popo National Park, 60 km southeast of Mexico City, at an altitude of 3985 m a.s.l. This station is part of the University Network of Atmospheric Observatories (http://www.ruoa.unam.mx) and comprises a complete set of in situ and meteorological instrumentation.

The measured spectra were analyzed with the retrieval code PROFFIT which uses the radiative transfer code PROF-FWD (Hase et al., 2004). For the calculation of the dry-air column-averaged mole fractions of carbon dioxide X_{CO_2}, CO$_2$ and O$_2$ were retrieved separately using a profile scaling procedure and with the microwindows and interfering species listed in Table 1. Pressure and temperature profiles from the National Centers for Environment Prediction (NCEP) were used, and the a priori profiles were obtained from the Whole Atmosphere Community Climate Model (WACCM). A single a priori profile of each retrieved species was used for the entire set of measurements.

3 Effect of the beam splitter on the retrieval

The TCCON instrumental requirements state that the network's necessary precision is best achieved using a CaF$_2$ beam splitter (TCCON-Wiki, 2010), but, in the case of the Altzomoni site, this would mean sacrificing routine measurements of spectra in the mid-infrared (200–3300 cm^{-1}) region since the beam splitter change needs to be performed manually. Given the location of the site and aside from complying with a long-term commitment with NDACC, it is of great interest to perform measurements of gases which absorb in the MIR region in order to characterize pollution transport
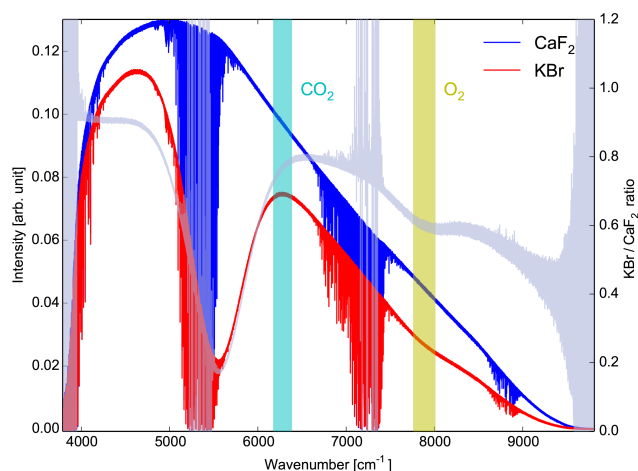
Figure 1. Spectra of a near-infrared (NIR) lamp measured with KBr (red) and CaF$_2$ (blue) beam splitters; the spectral regions where the CO$_2$ and O$_2$ target gases are retrieved are shown in cyan and yellow, respectively. The KBr / CaF$_2$ lamp intensity ratio, as shown in gray, is smooth at the target regions and is lower for O$_2$ (the gas which presents larger error differences among beam splitters).

Figure 2. Time series of the X_{CO_2} data set from the Altzomoni site (black points) with the elements of the KBr (red points) and the CaF$_2$ (blue points) ensembles. The inset plot show the SZA distribution of both ensembles.

events in the region and study the composition of the gases emitted by the active Popocatépetl volcano. For these reasons, a KBr beam splitter has been part of the configuration used at the site and the use of the CaF$_2$ beam splitter has been limited. Figure 1 shows two tungsten NIR lamp spectra, one measured with KBr (red) and another one with CaF$_2$ (blue), to illustrate the features of each measurement in the NIR region. The KBr spectra shows a slightly lower intensity and a dip on the 5000–6000 cm^{-1} spectral region. Kiel et al. (2016) showed that a small curvature might affect the retrieval results if no baseline is adjusted. The settings used for the retrievals of this study adjusted a smoothed baseline with 20 parameters for each microwindow used. The baseline curvature in the spectral region around the dip introduced by the KBr beam splitter is removed using a simplified radiometric calibration, assuming that the tungsten lamp produces a blackbody spectrum ($T = 1700$ K) and that there is no self-emission of the optical set-up in the spectral region above 4000 cm^{-1}. This calibration has a low impact on the columns (+0.021 % CO$_2$, +0.0053 % for O$_2$) due to the simultaneous fit of the baseline in the retrieval code.

In order to compare the impact of the KBr and CaF$_2$ beam splitters on the retrievals and since far more measurements are available with the KBr beam splitter (27 148) than with CaF$_2$ (2093), an ensemble of KBr measurements was formed reproducing the size and solar zenith angle (SZA) distribution of the CaF$_2$ measurements. A condition imposed was to only consider sets of consecutive measurements done within a 5 min lapse so that the precision of each retrieval product and SZA could be calculated. As shown in Fig. 2, the KBr ensemble consisted of measurements from 101 days between 30 July 2013 and 30 December 2015, while the CaF$_2$ ensem-
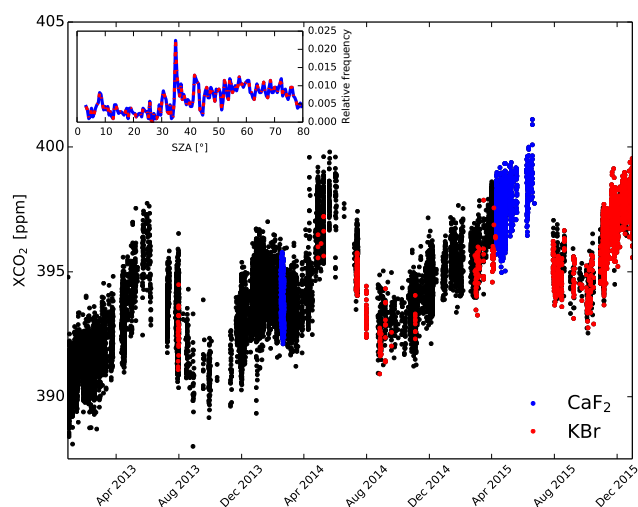
ble had measurements from 43 days from 15 February 2014 to 23 June 2015.

For the case of CO$_2$ column measurements, two references of precision exist: Rayner and O'Brien (2001) showed that a 0.25 % network precision would improve the current knowledge of the carbon cycle, while Olsen and Randerson (2004) suggested that a 0.1 % precision would allow an assessment of the strength of the carbon sink in the Northern Hemisphere. The following subsections are dedicated to determining where the Altzomoni data fall, using routinely a KBr beam splitter, in terms of these two benchmarks.

3.1 Retrieved CO$_2$ and O$_2$ error budgets

The error calculation implemented in PROFFIT allows one to estimate the errors associated with a total column retrieval (Barthlott et al., 2015). These include channeling and offset, instrumental line shape (ILS), temperature profile, line-of-sight (LOS), solar lines, spectroscopy and noise errors. The errors were calculated for each of the measurements that comprise the KBr and CaF$_2$ ensembles. The magnitude of the uncertainties and the statistical and systematic contributions for each source are listed in Table 2. The largest error difference between beam splitters is expected to originate from the noise for a given ensemble, since the spectral windows used for the retrievals are measured with a different signal-to-noise ratio (see Fig. 1). The purpose of obtaining the errors from the PROFFIT software was to determine the value of noise present in each measurement and how it depends on the beam splitter used. The noise calculation from PROFFIT takes into account the derivatives of the retrieval with respect of the measurement and the difference between the measurement and a simulated spectra from the forward model. Fig-

Table 2. Error sources used in the error estimation, the second column gives the uncertainty used and the third the statistical (Stat) and systematic (Sys) contributions of each source in percentage.

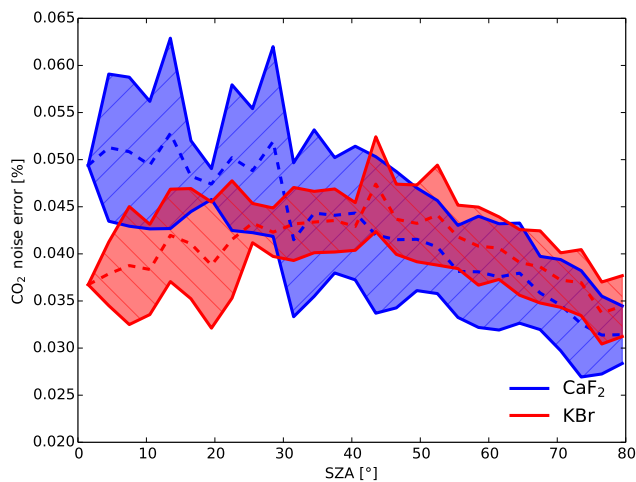| Error source	Uncertainty	Stat/Sys [%]
Baseline (offset/channeling)	0.1 %/0.2 %	50/50
ILS (modulation efficiency/ phase error)	2 %/0.01 rad	50/50
Line of sight	0.001 rad	90/10
Solar lines (intensity/scale)	1 %/1 × 10^{-6}	80/20
Temperature	1, 2 and 5 K	70/30
Spectroscopic parameters (S/γ)	2 %/5 %	0/100
Measurement noise	–	100/0

Figure 3. Mean noise error from PROFFIT for CO$_2$ total column as a function of SZA.

ures 3 and 4 show how the mean noise error from the CO$_2$ and the O$_2$ total columns depend on the beam splitter and the SZA, while Tables 3 and 4 show the mean values of each error source for two SZA values (20 and 70°). The noise error of the CO$_2$ column shows good agreement between beam splitters for SZAs above 30° but is lower in KBr measurements at smaller angles. For the O$_2$ column, the errors have similar behavior for angles below 30°, but the noise errors for angles above this value remain more or less constant and are 30–40 % larger for KBr than for CaF$_2$. Overall, the total statistical and systematic errors for both beam splitters estimated with this technique are quite similar.

3.2 Statistical precision from consecutive measurements

For a statistical estimation of the precision, we consider that the standard deviation of the consecutive measurements done within a 5 min lapse (typically 6 spectra) represents the overall precision of the measurements. This method is based on
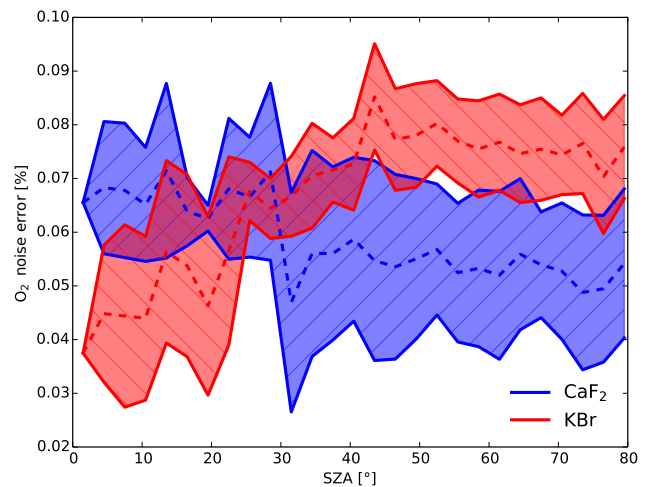

Figure 4. Mean noise error from PROFFIT for O$_2$ total column as a function of SZA.

the assumption that the actual gas columns undergo smaller changes in the short time considered than the measurement error. With the three products derived from an NIR measurement (CO$_2$ and O$_2$ columns and X_{CO_2}), three different precisions were calculated and used for estimating which part of the random error is independent from the CO$_2$ and O$_2$ columns and which part is correlated and thus cancels out when the X_{CO_2} ratio is calculated.

Assuming that the precisions of CO$_2$ and O$_2$ (σ_{CO_2} and σ_{O_2}) are due to both the noise and the correlated errors (see Eqs. 1 and 2) and the precision of X_{CO_2} depends only in the noise from both columns (Eq. 3), a system of equations was formed and solved using the mean precisions of the three products to obtain the mean correlated and noise errors of CO$_2$ and O$_2$ for each beam splitter.

$$\left(\sigma_{CO_2}\right)^2 = \left(\sigma^{\text{Correlated}}\right)^2 + \left(\sigma_{CO_2}^{\text{Noise}}\right)^2 \tag{1}$$

$$\left(\sigma_{O_2}\right)^2 = \left(\sigma^{\text{Correlated}}\right)^2 + \left(\sigma_{O_2}^{\text{Noise}}\right)^2 \tag{2}$$

$$\left(\sigma_{X_{CO_2}}\right)^2 = \left(\sigma_{CO_2}^{\text{Noise}}\right)^2 + \left(\sigma_{O_2}^{\text{Noise}}\right)^2 \tag{3}$$

As can be seen in the results from this exercise presented in Table 5, the mean noise errors from the columns are within the range of the values obtained using PROFFIT, and, in the case of X_{CO_2}, the mean value from all the KBr measurements in the ensemble was 25 % higher than with CaF$_2$. The contribution appears to be dominated by the noise in the O$_2$ retrieval. This is in accordance to the result in Sect. 3.1. However, as Fig. 5 shows, the mean X_{CO_2} precisions obtained from both beam splitters were below 0.1 %, and those of > 96 % of all the spectra in the ensemble measured with a KBr beam splitter fall below the 0.2 % value.

Table 3. Mean ensemble values of the statistical (Stat) and systematic (Sys) errors for 20 and 70° SZA (given in %) in CO$_2$ columns due to the assumed error sources of Table 2.

CO$_2$	SZA = 20°				SZA = 70°			
	KBr		CaF$_2$		KBr		CaF$_2$	
	Stat	Sys	Stat	Sys	Stat	Sys	Stat	Sys
Baseline	0.082	0.082	0.081	0.081	0.085	0.085	0.085	0.085
ILS	0.073	0.073	0.076	0.076	0.043	0.043	0.043	0.043
LOS	0.031	0.0035	0.031	0.0034	0.24	0.026	0.24	0.026
Solar lines	0.0071	0.0018	0.0092	0.0023	0.0065	0.0016	0.0082	0.0020
Temperature	0.019	0.0081	0.012	0.0053	0.031	0.013	0.032	0.014
Spectroscopy	–	2.13	–	2.16	–	2.13	–	2.13
Noise	0.039	–	0.047	–	0.037	–	0.035	–
Total	0.12	2.14	0.13	2.16	0.26	2.13	0.26	2.13

Table 4. Mean ensemble values of the statistical (Stat) and systematic (Sys) errors for 20 and 70° (given in %) in O$_2$ columns due to the assumed error sources of Table 2.

O$_2$	SZA = 20°				SZA = 70°			
	KBr		CaF$_2$		KBr		CaF$_2$	
	Stat	Sys	Stat	Sys	Stat	Sys	Stat	Sys
Baseline	0.090	0.090	0.087	0.087	0.089	0.089	0.090	0.090
ILS	0.060	0.060	0.059	0.059	0.032	0.032	0.032	0.032
LOS	0.031	0.0034	0.030	0.0033	0.22	0.025	0.22	0.024
Solar lines	0.0077	0.0019	0.0077	0.0019	0.0044	0.0011	0.0047	0.0012
Temperature	0.029	0.012	0.033	0.014	0.031	0.013	0.032	0.014
Spectroscopy	–	2.12	–	2.10	–	2.89	–	2.90
Noise	0.046	–	0.063	–	0.074	–	0.053	–
Total	0.13	2.12	0.13	2.10	0.25	2.89	0.25	2.90

Table 5. Mean precision, noise and correlation errors (given in %) for both ensembles, of 2093 measurements each, using KBr and CaF$_2$ beam splitters. The X_{CO_2} precision is the root-sum-square of the noise errors of CO$_2$ and O$_2$.

	σ_{CO_2}	σ_{O_2}	$\sigma^{\text{Correlated}}$	$\sigma_{CO_2}^{\text{Noise}}$	$\sigma_{O_2}^{\text{Noise}}$	σ_{XCO_2}
KBr	0.072 ± 0.0041	0.098 ± 0.0042	0.055 ± 0.0055	0.047 ± 0.0065	0.082 ± 0.0037	0.094 ± 0.0033
CaF$_2$	0.078 ± 0.0046	0.090 ± 0.0037	0.065 ± 0.0031	0.043 ± 0.0048	0.062 ± 0.0033	0.075 ± 0.0022

3.3 Bias estimation

The systematic difference between beam splitters was estimated for the three products obtained. Since there are no temporal coincidences between the measurements with both beam splitters, an independent set of measurements was used to calculate the bias. The ensembles were sorted in bins, so that the mean values of the data in each bin could be compared even if the measurements on the ensembles were not coincident in time.

For X_{CO_2}, the continuous data set of CO$_2$ in situ measurements from the Mauna Loa Observatory (MLO; 19.5362° N, 155.5763° W, 3397 m a.s.l.) was chosen, given the fact that both sites share a similar latitude and altitude. An in situ measurement in Altzomoni is now available, but the data does not cover the entire period of the FTIR ensemble. Although both data sets show a similar behavior, the purpose of using MLO in this context was to investigate the relative bias between both beam splitter ensembles with a common reference by arranging the data into bins. There were 189 coincidences for the KBr and 174 for CaF$_2$ data sets. The bias was obtained from the mean of the KBr–CaF$_2$ differences of these coincidences, sorted in 13 bins generated using the measurements in MLO. From the correlation plot for each beam splitter and a Bland–Altman plot (Bland and Altman, 1986) for
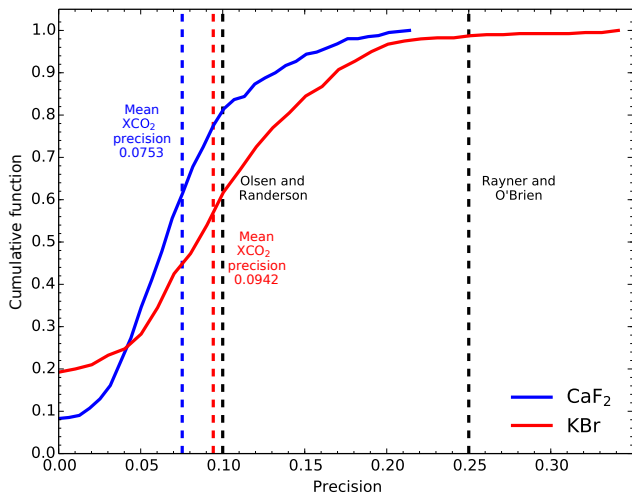
Figure 5. Cumulative function of X_{CO_2} precision for both beam splitters, with the blue and red dashed lines denoting the precision values from Table 5 obtained from the Sect. 3.2 approach. The black lines depict the existing precision goals for CO$_2$ found in the literature.

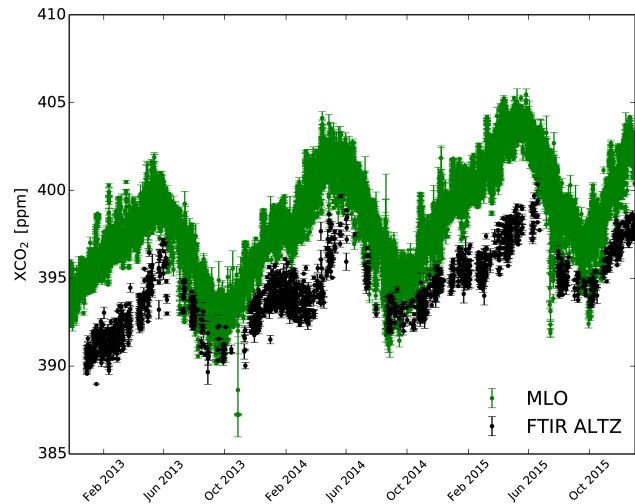**Figure 6.** Hourly means of Altzomoni X_{CO_2} (FTIR ALTZ, black points) and Mauna Loa Observatory in situ CO$_2$ (MLO, green points).

their differences shown in Fig. 7, a bias of $+0.14 \pm 0.064$ % is obtained for X_{CO_2}.

In the case of O$_2$ total columns, a bias was calculated by estimating the dry pressure column from surface pressure measurements at Altzomoni and the H$_2$O total columns retrieved in the NIR spectral region, which in turn was multiplied by the factor 0.2095 to convert to O$_2$ column. The number of coincidences obtained between the data sets was 100 for KBr and 110 for CaF$_2$. Figure 8 shows the plots and KBr–CaF$_2$ differences resulting in a bias of -0.17 ± 0.029 %.

The bias for CO$_2$ column was calculated from the biases obtained above (ΔX_{CO_2} and ΔO_2) using Eq. (4):

$$\Delta X_{CO_2} = \frac{\partial X_{CO_2}}{\partial CO_2} \cdot \Delta CO_2 + \frac{\partial X_{CO_2}}{\partial O_2} \cdot \Delta O_2, \qquad (4)$$

from which a value of $\Delta CO_2 = -0.030 \pm 0.070$ % is obtained. The biases and the mean values for each beam splitter are summarized in Table 6.

4 Observed time series

Figure 9 shows the daily means of the X_{CO_2} in black, derived from 29 241 measurements done in Altzomoni during 510 days between 28 December 2012 and 30 December 2015. A function was adjusted to the data using Eq. (5), taken from Wunch et al. (2013), where x is the decimal year and the obtained fitting parameters were as follows: $\alpha = 2.19$ ppm yr^{-1}, $a_0 = -0.0040$ ppm, $a_1 = -0.93$ ppm, $a_2 = 0.95$ ppm, $b_1 = 1.60$ ppm, and $b_2 = -0.54$ ppm. The linear term determines the trend of the series, which has the

value of 2.2 ppm yr^{-1}. The same function fitted over the MLO data set also shows a 2.2 ppm yr^{-1} trend.

$$f(x) = \alpha x + \sum_{k=0}^{2} a_k \cos(2\pi k x) + b_k \sin(2\pi k x) \qquad (5)$$

In Fig. 10, we present the X_{CO_2} and seasonally detrended X_{CO_2} averages showing a clear dependence with respect to the solar zenith angle. Although a treatment of the air mass dependence for X_{CO_2} has been considered following Dohe (2013) and Kiel et al. (2016), this may still not be fully corrected in the reported X_{CO_2}. However, a quantitative analysis correlating these observations with in situ measurements at Altzomoni, with a night-to-day average amplitude of approximately 5 ppm, indicates that carbon capture processes may be contributing significantly to the shown SZA dependence. The weekday averages were also calculated, and no distinct weekly pattern was detected from these data, which indicates that the measurements are representative for the free atmosphere and the influence of the nearby cities are minimal with respect to the total column.

5 Conclusions

Solar absorption FTIR measurements done with KBr and CaF$_2$ beam splitters were compared using equivalent ensembles containing more than 2000 spectra. The two methods used for evaluating the statistical errors gave similar results. In the case of CO$_2$ columns, the noise levels from the KBr measurements are on average 20 % lower than from CaF$_2$ measurements when solar zenith angles are below 30°. Measurements with larger SZAs have similar errors with both beam splitters. Larger error differences are encountered from

Table 6. Mean values of X_{CO_2}, CO$_2$ and O$_2$ and the bias obtained for each of them using the beam splitter ensembles. For X_{CO_2}, the Mauna Loa Observatory (MLO) was used, and for O$_2$ the dry pressure column was calculated and multiplied by 0.2095. The bias of CO$_2$ was obtained from Eq. (4).

|	KBr	CaF$_2$
X_{CO_2}		
Coincidences	189	174
Mean value FTIR (ppm)	396.07 ± 0.12	396.68 ± 0.14
Mean value MLO (ppm)	399.82 ± 0.14	402.04 ± 0.20
Mean difference (ppm)	-3.75 ± 0.077	-5.36 ± 0.11
Bias (KBr − CaF$_2$) (ppm)	$+0.56 \pm 0.25$ $(+0.14 \pm 0.064\%)$	
O$_2$		
Coincidences	100	110
Mean value FTIR (10^{24} molec cm^{-2})	2.90 ± 0.00089	2.90 ± 0.00077
Mean value dry pressure column (10^{24} molec cm^{-2})	2.82 ± 0.00055	2.82 ± 0.00046
Mean difference (10^{24} molec cm^{-2})	0.078 ± 0.00050	0.081 ± 0.00051
Bias (KBr − CaF$_2$) (10^{24} molec cm^{-2})	-0.0050 ± 0.00083 $(-0.17 \pm 0.029\%)$	
CO$_2$		
Mean value FTIR (10^{24} molec cm^{-2})	5.49 ± 0.00034	5.50 ± 0.00031
Bias (10^{24} molec cm^{-2})	-0.0016 ± 0.0039 $(-0.030 \pm 0.070\%)$	
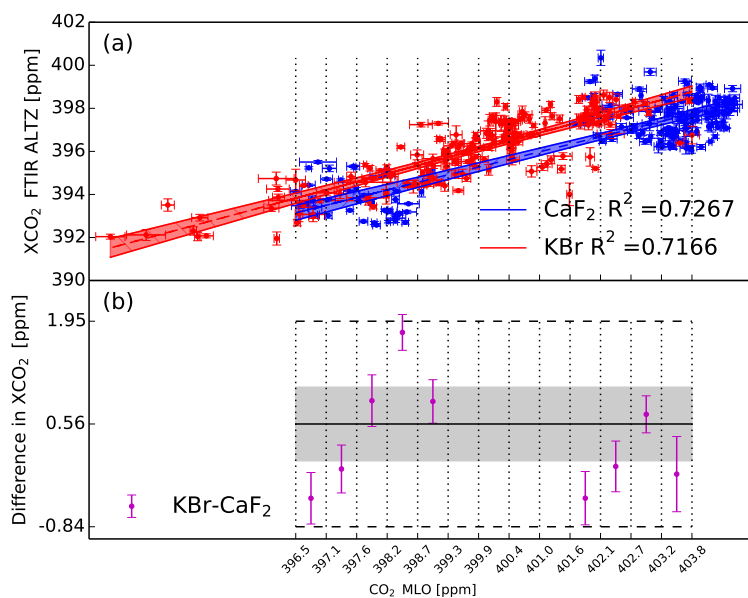
Figure 7. (a) shows the coincidences between the hourly means of the X_{CO_2} from the KBr (red) and CaF$_2$ (blue) ensembles and the CO$_2$ from the Mauna Loa Observatory (MLO) data set with a linear regression of the two sets, with the shaded area representing a 95 % confidence interval. **(b)** shows the difference of means of KBr and CaF$_2$ (purple points) for each bin (vertical lines) in a Bland–Altman plot, with the black dashed lines showing the standard deviation of all points. The black solid line represents the bias and the shaded area the standard error of the bias, both reported in Table 6.

the O$_2$ column retrievals. For angles below 30° the noise in KBr measurements is around 29 % lower but increases with the angle and remains constant above the CaF$_2$ levels, approximately 38 % higher.

Thus, in this study an estimation of the precision of each ensemble shows that the largest statistical error contribution in X_{CO_2} comes from the O$_2$ column retrieval. This outcome has the implication that column-averaged mixing ratios retrieved using KBr beam splitters have noise-related errors

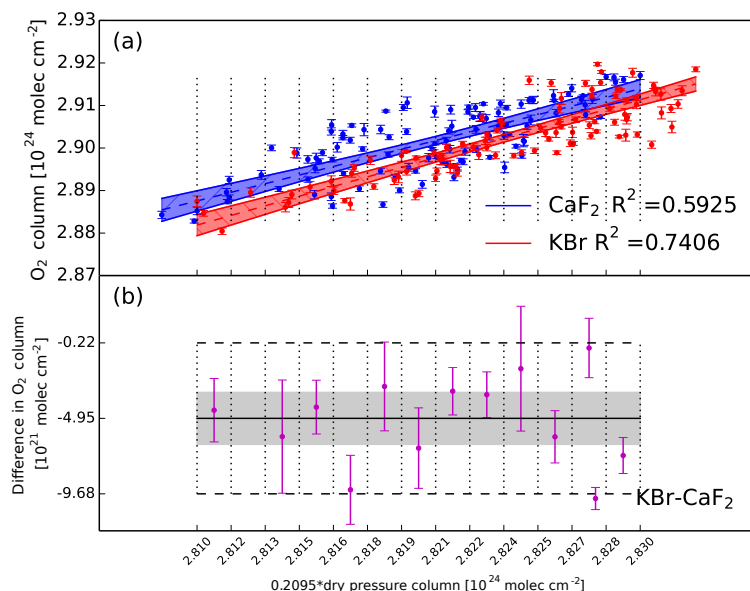**Figure 8. (a)** shows the coincidences between the hourly means of the O_2 from the KBr (red) and CaF_2 (blue) ensembles and the O_2 column obtained from the dry pressure column with a linear regression of the two sets, with the shaded area representing a 95 % confidence interval. **(b)** shows the difference of means of KBr and CaF_2 (purple points) for each bin (vertical lines) in a Bland–Altman plot, with the black dashed lines showing the standard deviation of all points. The black solid line represents the bias and the shaded area the standard error of the bias, both reported in Table 6.
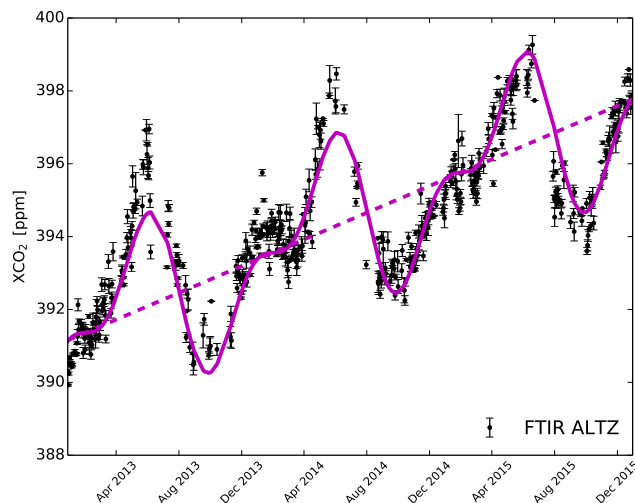
Figure 9. Daily means of the X_{CO_2} data set from the Altzomoni site (black points). The purple solid line is a curve adjusted to the series (see text) with a linear term, represented by the dashed line, of 2.2 ppm yr^{-1}, which is the trend for this 3-year period.

Figure 10. (a) shows X_{CO_2} from the Altzomoni site as a function of solar zenith angle. **(b)** shows the seasonally detrended X_{CO_2} using the coefficients obtained for Eq. (5). The solid lines represent mean values and the dashed lines standard deviations.

which are on average about 25 % larger than with CaF_2. However, mean X_{CO_2} precision was found to be below 0.1, and > 96 % of the measurements made with both optical configurations fall well below the 0.2 % precision.

These results provide enough evidence that measurements performed with a KBr beam splitter are reliable and useful for carbon cycle studies. This includes all FTIR instruments
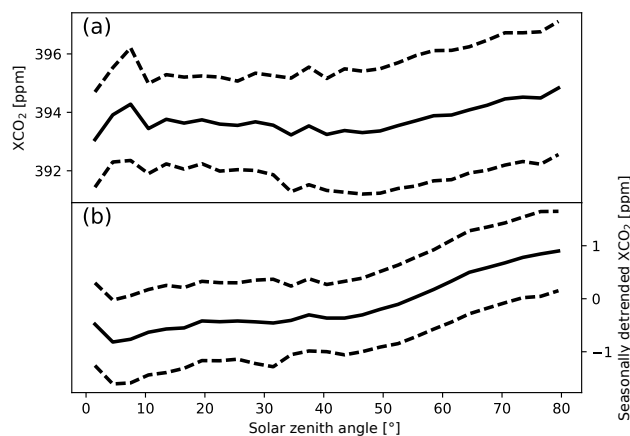
which are committed to complying with NDACC requirements and have an additional InGaAs detector available for NIR spectral measurements. A larger number of sites producing confident X_{CO_2} data sets would allow us to increase our current knowledge of the variability of this important greenhouse gas.

When doing direct comparisons across a network or using single retrievals for intercomparing timed observations, however, one needs to be cautious and consider a possible bias.

We have estimated a bias of 0.14 % for X_{CO_2} between beam splitters using data from the Mauna Loa Observatory.

A rich data set of X_{CO_2} was put together from more than 3 years of measurements in central Mexico. A very distinct annual cycle was identified with an amplitude of ~ 6 ppm and a positive trend of 2.2 ppm yr^{-1}.

Competing interests. The authors declare that they have no conflict of interest.

Edited by: Hal Maring
Reviewed by: Paul O. Wennberg and one anonymous referee

References

Báez, A., Reyes, M., Rosas, I., and Mosino, P.: CO$_2$ concentrations in the highly polluted atmosphere of Mexico City, Atmósfera, 1, available at: http://www.revistascca.unam.mx/atm/index.php/atm/article/view/8271 (last access: 20 December 2016), 1988.

Barthlott, S., Schneider, M., Hase, F., Wiegele, A., Christner, E., González, Y., Blumenstock, T., Dohe, S., García, O. E., Sepúlveda, E., Strong, K., Mendonca, J., Weaver, D., Palm, M., Deutscher, N. M., Warneke, T., Notholt, J., Lejeune, B., Mahieu, E., Jones, N., Griffith, D. W. T., Velazco, V. A., Smale, D., Robinson, J., Kivi, R., Heikkinen, P., and Raffalski, U.: Using X_{CO_2} retrievals for assessing the long-term consistency of NDACC/FTIR data sets, Atmos. Meas. Tech., 8, 1555–1573, https://doi.org/10.5194/amt-8-1555-2015, 2015.

Bland, J. M. and Altman, D.: Statistical methods for assessing agreement between two methods of clinical measurement, Lancet, 327, 307–310, https://doi.org/10.1016/S0140-6736(86)90837-8, 1986.

Chahine, M. T., Chen, L., Dimotakis, P., Jiang, X., Li, Q., Olsen, E. T., Pagano, T., Randerson, J., and Yung, Y. L.: Satellite remote sounding of mid-tropospheric CO$_2$, Geophys. Res. Lett., 35, 117807, https://doi.org/10.1029/2008GL035022, 2008.

Crevoisier, C., Chédin, A., Matsueda, H., Machida, T., Armante, R., and Scott, N. A.: First year of upper tropospheric integrated content of CO$_2$ from IASI hyperspectral infrared observations, Atmos. Chem. Phys., 9, 4797–4810, https://doi.org/10.5194/acp-9-4797-2009, 2009.

Dohe, S.: Measurements of atmospheric CO$_2$ columns using ground-based FTIR spectra, PhD thesis, Karlsruher Institut für Technologie (KIT), Karlsruhe, Germany, 2013.

Foucher, P. Y., Chédin, A., Armante, R., Boone, C., Crevoisier, C., and Bernath, P.: Carbon dioxide atmospheric vertical profiles retrieved from space observation using ACE-FTS solar occultation instrument, Atmos. Chem. Phys., 11, 2455–2470, https://doi.org/10.5194/acp-11-2455-2011, 2011.

Gisi, M., Hase, F., Dohe, S., and Blumenstock, T.: Camtracker: a new camera controlled high precision solar tracker system for FTIR-spectrometers, Atmos. Meas. Tech., 4, 47–54, https://doi.org/10.5194/amt-4-47-2011, 2011.

Grutter, M.: Multi-Gas analysis of ambient air using FTIR spectroscopy over Mexico City, Atmósfera, 16, available at: http://www.revistascca.unam.mx/atm/index.php/atm/article/view/8506 (last access: 19 December 2016), 2003.

Hartmann, D., Klein Tank, A., Rusticucci, M., Alexander, L., Brönnimann, S., Charabi, Y., Dentener, F., Dlugokencky, E., Easterling, D., Kaplan, A., Soden, B., Thorne, P., Wild, M., and Zhai, P.: Observations: Atmosphere and Surface, in: Climate Change 2013: The Physical Science Basis, Contribution of Working Group I to the Fifth Assessment Report of the Intergovernmental Panel on Climate Change, book section 2, edited by: Stocker, T., Qin, D., Plattner, G.-K., Tignor, M., Allen, S., Boschung, J., Nauels, A., Xia, Y., Bex, V., and Midgley, P., Cambridge University Press, Cambridge, UK and New York, NY, USA, 159–254, https://doi.org/10.1017/CBO9781107415324.008, 2013.

Hase, F., Hannigan, J., Coffey, M., Goldman, A., Höpfner, M., Jones, N., Rinsland, C., and Wood, S.: Intercomparison of retrieval codes used for the analysis of high-resolution, ground-based FTIR measurements, J. Quant. Spectrosc. Ra., 87, 25–52, https://doi.org/10.1016/j.jqsrt.2003.12.008, 2004.

Kiel, M., Wunch, D., Wennberg, P. O., Toon, G. C., Hase, F., and Blumenstock, T.: Improved retrieval of gas abundances from near-infrared solar FTIR spectra measured at the Karlsruhe TCCON station, Atmos. Meas. Tech., 9, 669–682, https://doi.org/10.5194/amt-9-669-2016, 2016.

Kulawik, S. S., Jones, D. B. A., Nassar, R., Irion, F. W., Worden, J. R., Bowman, K. W., Machida, T., Matsueda, H., Sawa, Y., Biraud, S. C., Fischer, M. L., and Jacobson, A. R.: Characterization of Tropospheric Emission Spectrometer (TES) CO$_2$ for carbon cycle science, Atmos. Chem. Phys., 10, 5601–5623, https://doi.org/10.5194/acp-10-5601-2010, 2010.

Kuze, A., Suto, H., Nakajima, M., and Hamazaki, T.: Thermal and near infrared sensor for carbon observation Fourier-transform spectrometer on the Greenhouse Gases Observing Satellite for greenhouse gases monitoring, Appl. Optics, 48, 6716–6733, https://doi.org/10.1364/AO.48.006716, 2009.

Myhre, G., Shindell, D., Bréon, F.-M., Collins, W., Fuglestvedt, J., Huang, J., Koch, D., Lamarque, J.-F., Lee, D., Mendoza, B., Nakajima, T., Robock, A., Stephens, G., Takemura, T., and Zhang, H.: Anthropogenic and Natural Radiative Forcing, in: Climate Change 2013: The Physical Sci-

ence Basis, Contribution of Working Group I to the Fifth Assessment Report of the Intergovernmental Panel on Climate Change, book section 8, edited by: Stocker, T., Qin, D., Plattner, G.-K., Tignor, M., Allen, S., Boschung, J., Nauels, A., Xia, Y., Bex, V., and Midgley, P., Cambridge University Press, Cambridge, UK and New York, NY, USA, 659–740, https://doi.org/10.1017/CBO9781107415324.018, 2013.

Olsen, S. C. and Randerson, J. T.: Differences between surface and column atmospheric CO_2 and implications for carbon cycle research, J. Geophys. Res.-Atmos., 109, d02301, https://doi.org/10.1029/2003JD003968, 2004.

Rayner, P. J. and O'Brien, D. M.: The utility of remotely sensed CO_2 concentration data in surface source inversions, Geophys. Res. Lett., 28, 175–178, https://doi.org/10.1029/2000GL011912, 2001.

Reuter, M., Bovensmann, H., Buchwitz, M., Burrows, J. P., Connor, B. J., Deutscher, N. M., Griffith, D. W. T., Heymann, J., Keppel-Aleks, G., Messerschmidt, J., Notholt, J., Petri, C., Robinson, J., Schneising, O., Sherlock, V., Velazco, V., Warneke, T., Wennberg, P. O., and Wunch, D.: Retrieval of atmospheric CO_2 with enhanced accuracy and precision from SCIAMACHY: Validation with FTS measurements and comparison with model results, J. Geophys. Res.-Atmos., 116, d04301, https://doi.org/10.1029/2010JD015047, 2011.

TCCON-Wiki: TCCON Requirements, available at: https://tccon-wiki.caltech.edu/Network_Policy/Data_Protocol (last access: 19 December 2016), 2010.

Velasco, E., Pressley, S., Allwine, E., Westberg, H., and Lamb, B.: Measurements of {CO_2} fluxes from the Mexico City urban landscape, Atmos. Environ., 39, 7433–7446, https://doi.org/10.1016/j.atmosenv.2005.08.038, 2005.

Velasco, E., Pressley, S., Grivicke, R., Allwine, E., Coons, T., Foster, W., Jobson, B. T., Westberg, H., Ramos, R., Hernández, F., Molina, L. T., and Lamb, B.: Eddy covariance flux measurements of pollutant gases in urban Mexico City, Atmos. Chem. Phys., 9, 7325–7342, https://doi.org/10.5194/acp-9-7325-2009, 2009.

WMO: The Global Atmospheric Watch Programme: 17th WMO/IAEA Meeting on Carbon Dioxide, Other Greenhouse Gases and Related Tracers Measurement Techniques (GGMT-2013), Beijing, China, 10–13 June 2013, GAW Report No. 213, World Meteorological Organization, Geneva, Switzerland, 2014.

Wunch, D., Toon, G. C., Blavier, J.-F. L., Washenfelder, R. A., Notholt, J., Connor, B. J., Griffith, D. W. T., Sherlock, V., and Wennberg, P. O.: The Total Carbon Column Observing Network, Philos. T. Roy. Soc. Lond. A, 369, 2087–2112, https://doi.org/10.1098/rsta.2010.0240, 2011.

Wunch, D., Wennberg, P. O., Messerschmidt, J., Parazoo, N. C., Toon, G. C., Deutscher, N. M., Keppel-Aleks, G., Roehl, C. M., Randerson, J. T., Warneke, T., and Notholt, J.: The covariation of Northern Hemisphere summertime CO_2 with surface temperature in boreal regions, Atmos. Chem. Phys., 13, 9447–9459, https://doi.org/10.5194/acp-13-9447-2013, 2013.

Wunch, D., Wennberg, P. O., Osterman, G., Fisher, B., Naylor, B., Roehl, C. M., O'Dell, C., Mandrake, L., Viatte, C., Kiel, M., Griffith, D. W. T., Deutscher, N. M., Velazco, V. A., Notholt, J., Warneke, T., Petri, C., De Maziere, M., Sha, M. K., Sussmann, R., Rettinger, M., Pollard, D., Robinson, J., Morino, I., Uchino, O., Hase, F., Blumenstock, T., Feist, D. G., Arnold, S. G., Strong, K., Mendonca, J., Kivi, R., Heikkinen, P., Iraci, L., Podolske, J., Hillyard, P. W., Kawakami, S., Dubey, M. K., Parker, H. A., Sepulveda, E., García, O. E., Te, Y., Jeseck, P., Gunson, M. R., Crisp, D., and Eldering, A.: Comparisons of the Orbiting Carbon Observatory-2 (OCO-2) X_{CO_2} measurements with TCCON, Atmos. Meas. Tech., 10, 2209–2238, https://doi.org/10.5194/amt-10-2209-2017, 2017.